

## Charge optimized many-body potential for the Si/SiO<sub>2</sub> system

Jianguo Yu, Susan B. Sinnott, and Simon R. Phillpot

*Department of Materials Science and Engineering, University of Florida, Gainesville, Florida 32611-6400, USA*

(Received 17 October 2006; revised manuscript received 22 December 2006; published 9 February 2007)

A dynamic-charge, many-body potential for the Si/SiO<sub>2</sub> system, based on an extended Tersoff potential for semiconductors, is proposed and implemented. The validity of the potential function is tested for both pure silicon and for five polymorphs of silica, for which good agreement is found between the calculated and experimental structural parameters and energies. The dynamic charge transfer intrinsic to the potential function allows the interface properties to be captured automatically, as demonstrated for the silicon/ $\beta$ -cristobalite interface.

DOI: [10.1103/PhysRevB.75.085311](https://doi.org/10.1103/PhysRevB.75.085311)

PACS number(s): 61.43.Bn, 61.82.Fk, 68.05.Cf, 68.18.Fg

### I. INTRODUCTION

Silicon (Si) and silicon oxides (SiO<sub>2</sub>) are the key elements of the silicon metal-oxide semiconductor (MOS)/complementary metal-oxide semiconductor (CMOS) gates used in today's transistors; as such, they are one of the most heavily studied material systems.<sup>1</sup> As an essential part of MOS devices, a high-quality Si/SiO<sub>2</sub> interface can be easily formed by thermal oxidation.<sup>2</sup> With the continued reduction in device size according to Moore's Law,<sup>3</sup> the atomic structure of the Si/SiO<sub>2</sub> interface becomes ever more critical to device performance.

Atomistic computational methods, such as quantum-chemical and electronic-structure methods, tight-binding approaches, and many-body empirical potentials, have played an important role in developing an understanding of these new nanometer-scale components. Although the length scales on which experimental devices are built are still larger than the scales at which atomic-scale calculations and simulations can be carried out, as feature sizes continue to shrink and computer power continues to increase, it will soon be feasible to model a nanometer-scale device completely atomistically based on empirical many-body potentials. The objective of the present work is to build a flexible, empirical potential framework for the Si/SiO<sub>2</sub> system suited to such large-scale simulations.

The nature of the covalent bonding in Si often makes the description of complicated phenomena difficult. Many different methods can be used to model covalent bonding, including empirical potentials, although *ab initio* quantum-mechanical<sup>4</sup> and density-functional theory (DFT) (Refs. 5 and 6) calculations are generally the most accurate and robust. Similarly, silica is one of the most difficult materials to model due to its structural complexity and the subtlety of the energy differences among its various polymorphs. Although an accurate prediction of the phase equilibrium between the different silica polymorphs can be predicted by electronic structure methods,<sup>7</sup> these approaches are generally too computationally intensive to be used to study interfacial structures without introducing significant strain.<sup>8</sup> Furthermore, the time scales of most dynamical processes of interest are still prohibitively large for *ab initio* molecular-dynamics (MD) simulations.<sup>9,10</sup> Thus there is tremendous incentive to develop robust empirical schemes to model life-sized Si/SiO<sub>2</sub> interfacial systems.

A number of empirical potentials have been proposed and applied to silicon, including the Stillinger-Weber (SW),<sup>11</sup> Biswas-Hamann,<sup>12</sup> Tersoff<sup>13-15</sup> and EDIP (Ref. 16) potentials. Among these potentials, Tersoff<sup>13-15</sup> is one of the most widely used. It consists of many-body interactions, allows for bond breaking and new bond formation, and has been applied successfully to study a wide range of properties such as phonon propagation,<sup>17</sup> thermomechanical responses,<sup>18</sup> point defect stability,<sup>13</sup> noncrystal phases,<sup>13</sup> Si adatom adsorption and diffusion,<sup>19</sup> and Si adatom epitaxial growth.<sup>20</sup>

Meanwhile many force field potentials have been constructed for silica systems, including the TTAM potential,<sup>21</sup> the BKS potential,<sup>22</sup> the extended SW Si potential,<sup>23</sup> the extended semiconductor Tersoff potential,<sup>24</sup> and the *ab initio* derived augmented Tersoff potential.<sup>25</sup> In order to capture the largely ionic nature of the interactions in SiO<sub>2</sub>, fixed-charge Coulomb interactions are also taken into account by some potentials, such as TTAM (Ref. 21) and BKS.<sup>22</sup> Though fixed charge schemes work well for bulklike systems, they are generally less robust in systems that are far from bulklike or that require charge adjustment in response to changing system conditions. Recently, a more flexible and sophisticated reactive force field (ReaxFF) method was implemented by Goddard and co-workers<sup>26</sup> for the Si/SiO<sub>2</sub> system and more complex reactive systems, in which atomic charges are allowed to change dynamically with the changing atomic environment.

Although the above potentials and many others have been successful in describing interactions in Si and SiO<sub>2</sub> systems separately, only a few potentials (e.g., Refs. 23-26) are applicable to Si/SiO<sub>2</sub> interfaces. However, since they are non-charged potentials, the extended SW Si potential<sup>23</sup> and the augmented Tersoff potential<sup>25</sup> do not address the charge redistribution issue. The ReaxFF method<sup>26</sup> is a variable charge transfer scheme that forms a strong bridge between quantum chemical and empirical force field calculations. However, the application of the ReaxFF method to large-scale systems may be limited due to the fact that it requires a significantly larger computational effort than traditional empirical force field schemes.

The extended Tersoff potential<sup>24</sup> is also a variable charge scheme. In particular, Yasukawa<sup>24</sup> extended the bond-order method of Tersoff to the Si/SiO<sub>2</sub> system by including self-consistent charge determination and an electrostatic term in the spirit of the Rappe and Goddard approach,<sup>27</sup> which was

also used for Al/Al<sub>2</sub>O<sub>3</sub> by Streitz and Mintmire.<sup>28</sup> The replacement of the metallic EAM terms of the Streitz and Mintmire approach by the covalent terms of Tersoff is quite reasonable since Brenner showed some time ago that in the appropriate limit, they are formally identical.<sup>29</sup> While Yasukawa applied his approach to the Si/SiO<sub>2</sub> system, Iwasaki and Miura<sup>30</sup> explicitly showed its ability to simulate metal-ceramic interfaces. For example, they determined the adhesion energy of Al/TiN, Cu/TiN, Cu/W, and Al/W interfaces and found their relative values to be in excellent agreement with experiment.<sup>30</sup>

In this paper, we build on the Yasukawa approach to develop a robust potential to facilitate the life-sized, atomic-level simulation of the Si/SiO<sub>2</sub> system. This charge-optimized many-body (COMB) approach takes into account the effect of charge transfer using both the electronegativity equalization principle and many-body interactions. Its validity is tested for the Si and SiO<sub>2</sub> systems. Specifically, the structural properties and relative energies for silicon and a variety of silica polymorphs are obtained and found to compare extremely well with experimental results. Moreover, with the capability of dynamic charge transfer as an intrinsic feature of the potential function, properties such as the substoichiometric oxide in the interface layers between silicon and silicon oxides should also be captured automatically. The results for a strained interface between silicon and  $\beta$ -cristobalite ( $\beta$ -C) confirm this expectation.

The rest of this paper is organized as follows. The charge-optimized many-body potentials are described in Sec. II. The Yasukawa potential function and test results will be presented in Sec. III. The COMB06 potential for silicon and silica polymorphs are given in Sec. IV. The demonstration of its ability to describe the Si/SiO<sub>2</sub> interface is given in Sec. V. Section VI contains conclusions.

## II. CHARGE-OPTIMIZED MANY-BODY POTENTIALS

In standard MD simulations of systems subject to electrostatic forces, the charge on each ion is fixed. Such fixed charge schemes have several limitations, the most important of which is the inability to the system to redistribute charge in a physically realistic manner in cases that are far from the ideal bulklike state. To take a trivial example, the charge states of H and Cl atoms change considerably as they approach each other to form a HCl molecule. A second, more subtle, example is ferroelectric PbTiO<sub>3</sub>, which undergoes a transition from the paraelectric cubic phase to the ferroelectric tetragonal phase. During this phase transition, the charge state of the ions, particularly the Pb ions, changes considerably. While these necessary charge redistributions take place naturally in an electronic structure calculation, special methods must be used in atomic-level simulations to enable this process to occur.

The first atomic-level charge-transfer methods that incorporated such effects were those of Rappe and Goddard,<sup>27</sup> and Streitz and Mintmire.<sup>28</sup> The key concept in such charge-transfer methods is that the charge state is determined in a self-consistent manner. In particular, in the Rappe-Goddard method, the self-energy of an ion is defined as

$$E_i^S(q_i) = \chi_i q_i + \frac{1}{2} J_i q_i^2, \quad (1)$$

in which  $\chi_i$  is the electronegativity of the  $i$ th atom (a purely atomic, environment independent quantity),  $J_i$  is the self-Coulomb repulsion (atomic hardness) of the  $i$ th atom, and  $q_i$  is the charge of atom  $i$ . Although the functional form in Eq. (1) has been widely adopted in charge transfer methods, it is not the only possible choice. Indeed, we will see that a judicious modification of the form  $E_i^S(q_i)$  can actually yield better materials fidelity.

The contribution to the total potential energy of the system coming from the interatomic interactions can be written in the charge-dependent general form as the sum of the self energy and of the potential energy arising from the interactions among atoms and ions:  $E_T(\{q_i\}, \{r_{ij}\}) = E_i^S(\{q_i\}) + V(\{q_i\}, \{r_{ij}\})$ . The functional form of  $E_T$  depends on the specific method, taking different forms, for example, in the Streitz-Mintmire approach for the Al/Al<sub>2</sub>O<sub>3</sub> system,<sup>28</sup> and in the Yasukawa approach for Si/SiO<sub>2</sub>,<sup>24</sup> which forms the foundation of the work described in this paper.

In particular, all of these approaches can be considered to be members of a family of potentials that include both charge-transfer and the many-body interactions needed to capture the complexities of bonding in metals, ionic materials, and covalent materials. We denote such potentials as charge-optimized many-body (COMB) potentials. Regardless of the specific functional form of a COMB potential, the key task of the simulation is to correctly determine both the atoms positions and their charges. The traditional method to do this is via a self-consistency loop at every step, which brings all the charges to their equilibrium values. However, this is very slow as, for a system of  $N$  ions, it involves taking the inverse of an  $N$  by  $N$  matrix, a task that typically scales as  $O(N^2)$ , thus quickly becoming computationally impractical as system size  $N$  increases. To bypass this computational bottleneck, and building on the extended-Lagrangian approach used for constant stress<sup>31</sup> and constant temperature,<sup>32</sup> Rick *et al.*<sup>33</sup> defined an effective Lagrangian approach in which the charges are treated as dynamical variables that can evolve explicitly in time. The kinetic energy of such a dynamical system is given by  $T$ , where

$$T = \frac{1}{2} \sum_i m_i \dot{r}_i^2 + \frac{1}{2} \sum_i s_i \dot{q}_i^2. \quad (2)$$

The first term is the familiar kinetic energy term associated with the physical movement of atoms. The second term is a fictional kinetic energy term associated with dynamical changes in the charges of the atoms;  $s_i$  is the effective inertia of an ion to changes in its charge state. The Lagrangian  $L$  for this classical mechanical system is  $L = T - E_T$ . Equations of motion for the positions and charges of the atoms can be determined from the Euler-Lagrange equations<sup>34</sup> to be

$$m_i \ddot{r}_i = - \frac{\partial}{\partial r_i} E_T(\{r_{ij}\}, \{q_{ij}\}), \quad (3)$$

$$s_i \ddot{q}_i = - \frac{\partial}{\partial q_i} E_T(\{r_i\}, \{q_i\}). \quad (4)$$

Here  $m_i$ ,  $\mathbf{r}_i$ , and  $q_i$  are the atomic mass, atomic position, and atomic charge of the  $i$ th atom. In this method, the individual charges respond to deviations from the electronegativity equalization by moving toward a new charge, which more closely satisfies the equalization condition. These equations can be evolved with standard integration schemes such as the Verlet algorithm.<sup>35</sup> Most importantly, by replacing the matrix-based method for determining the charge, the code remains  $O(N)$ , a crucial requirement for large-scale simulations. An additional advantage from a computational viewpoint is that the total-energy function  $E = T + E_T$  is conserved.

In general the method of dynamic charge transfer involves rigorously imposing the electronegativity equalization condition at each step in the MD simulation. For the case in which a system has no charge exchange with environment, the total charge is constant,  $C$  (usually  $C=0$ ):

$$\sum_i^N q_i = C. \quad (5)$$

Combining this holonomic constraint, i.e., the condition of the total charged be conserved, the set of local atomic charges,<sup>26</sup> are determined by requiring that they minimize the total potential energy  $E_T$ . This minimization condition is equivalent to the electronegativity equalization condition that all the electrostatic chemical potentials are equal.

The local electrostatic chemical potential  $\mu_i$  is defined as<sup>27</sup>

$$\mu_i = \frac{\partial E_T}{\partial q_i}, \quad (6)$$

where  $e$  is the elementary charge. Thus the equalization condition may be written as<sup>27</sup>

$$\mu_i = \bar{\mu} = \frac{1}{N} \sum_i \mu_i, \quad (7)$$

where  $N$  is the system atom number and  $\bar{\mu}$  is the average electrostatic chemical potential of the  $N$  atom system. In particular, the electrostatic chemical potential equalization condition is equivalent to stating that the driving force to shift charge from one atom to another is zero. Thus the equation of motion for charges is governed by<sup>33</sup>

$$-m_q \ddot{q}_i = \mu_i - \bar{\mu}. \quad (8)$$

Since the specific values of the effective inertias of the charges,  $\{s_i\}$ , should not be too important, it is convenient to have one value for all atoms in the system ( $s_i = m_q$ ).

In order to achieve an efficient charge convergence between each step in the MD simulation, it is convenient to depart from a strictly Lagrangian approach by adding a damping term to the dynamical charge transfer scheme:

$$-m_q \ddot{q}_i = \mu_i - \bar{\mu} + \eta_d \dot{q}_i, \quad (9)$$

where  $\eta_d$  is the damping factor, which can be optimized on a case-by-case basis.

A dynamical approach very similar to this was also explored by Keffer and Mintmire.<sup>36</sup> However, they pointed out that it could lead to instabilities when performed in the strictly Lagrangian framework. We find that when implemented with a damping term as in Eq. (9), the system is stable. Of course, the addition of this damping term also means that there is no conserved energy in the simulation.

### III. YASUKAWA COMB POTENTIAL

The underpinning of any MD simulation is the interatomic potential, with the quality of the simulation results being determined by the materials fidelity of the potential. Generally, more functional complex potentials can, with appropriate parametrization, reproduce a wider range of physical behaviors of a system, albeit often with an undesirable increase in the computational load.

#### A. Yasukawa's potential

The widely used Tersoff potentials for semiconductors were developed by taking into account the effects of coordination-number changes on the local short-range environment of the covalent bonds. For the case of materials containing ions of different species, the effects of charge transfer also play an important role. Yasukawa's potential<sup>24</sup> was developed by adding terms corresponding to the effects of charge transfer to the original Tersoff potential. The potential function has the general form

$$E_T = \sum_i E_i = \sum_i \left[ E_i^S + \frac{1}{2} \sum_{j \neq i} V_{ij}(r_{ij}, q_i, q_j) \right]. \quad (10)$$

Here  $E_i$  is the potential for atom  $i$ ,  $E_i^S(q_i)$  is the previously defined self-energy term [Eq. (1)],  $V_{ij}$  is the interatomic potential between the  $i$ th and  $j$ th atoms, and  $r_{ij}$  is the distance between atoms  $i$  and  $j$ . In the Yasukawa potential, the interaction potential energy  $V_{ij}$  consists of four components:  $U_{ij}^R$ ,  $U_{ij}^A$ ,  $U_{ij}^I$ , and  $U_{ij}^V$  which are the repulsive energy, the short-range attractive energy, the ionic bond energy, and van der Waals energy, respectively, and are defined as

$$V_{ij}(r_{ij}, q_i, q_j) = U_{ij}^R(r_{ij}) + U_{ij}^A(r_{ij}, q_i, q_j) + U_{ij}^I(r_{ij}, q_i, q_j) + U_{ij}^V(r_{ij}), \quad (11)$$

$$U_{ij}^R(r_{ij}) = f_{S_{ij}} A_{ij} e^{(-\lambda_{ij} r_{ij})}, \quad (12)$$

$$U_{ij}^A(r_{ij}, q_i, q_j) = -f_{S_{ij}} b_{ij} B_{ij} e^{(-\alpha_{ij} r_{ij})}, \quad (13)$$

$$U_{ij}^I(r_{ij}, q_i, q_j) = f_{L_{ij}} \eta_i \eta_j q_i q_j / (4\pi\epsilon_0 r_{ij}), \quad (14)$$

$$U_{ij}^V(r_{ij}) = f_{L_{ij}} (C_{VDW_i} C_{VDW_j})^{1/2} / r_{ij}^6. \quad (15)$$

In Eq. (14),  $\epsilon_0$  is the permittivity of free space. The three-body effects are incorporated into the bond-order factors  $b_{ij}$  in the short-range attractive energy term as

$$b_{ij} = \left[ 1 + \left( \beta_i \sum_{k \neq i, j} \zeta_{ijk} g(\theta_{jik}) \right)^{n_i} \right]^{-1/2 n_i}, \quad (16)$$

where

$$\zeta_{ijk} = f_{S_{ik}} e^{[\alpha_{ij}^m (r_{ij} - r_{ik})^{m_i}]}, \quad (17)$$

$$g(\theta_{jik}) = 1 + \frac{c_i^2}{d_i^2} - \frac{c_i^2}{d_i^2 + (h_i - \cos \theta_{jik})^2}, \quad (18)$$

in which  $\theta_{jik}$  is the angle between bonds  $ij$  and  $ik$ . The potential is smoothly cut off by cutoff functions, defined as

$$f_{S_{ij}} = f_c[r_{ij}, (R_S R_{S_j})^{1/2}, (S_S S_{S_j})^{1/2}], \quad (19)$$

$$f_{L_{ij}} = f_c[r_{ij}, (R_L R_{L_j})^{1/2}, (S_L S_{L_j})^{1/2}], \quad (20)$$

$$f_c(r, R, S) = \begin{cases} 1 & r \leq R \\ \frac{1}{2} \left[ 1 + \cos \left( \pi \frac{r-R}{S-R} \right) \right] & R < r < S \\ 0 & r \geq S \end{cases}, \quad (21)$$

where  $R$  and  $S$  are appropriate cutoff radii.

The inverse decay lengths  $\lambda_{ij}$  and  $\alpha_{ij}$ , the coefficients  $A_{ij}$  and  $B_{ij}$  depend only on the types of the interacting atoms and may be expressed as

$$\lambda_{ij} = (\lambda_i + \lambda_j)/2, \quad (22)$$

$$\alpha_{ij} = (\alpha_i + \alpha_j)/2, \quad (23)$$

$$A_{ij} = \sqrt{A_S A_{S_j}}, \quad (24)$$

$$B_{ij} = \sqrt{B_S B_{S_j}}. \quad (25)$$

The coefficients  $A_{S_i}$  and  $B_{S_i}$  depend on the charge of the  $i$ th atom:

$$A_{S_i} = A_i e^{(\lambda_i D_i)}, \quad (26)$$

$$B_{S_i} = B_i e^{(\alpha_i D_i)} [a_{B_i} - |b_{B_i} (q_i - Q_{O_i})|^{n_{B_i}}], \quad (27)$$

$$D_i = D_{U_i} + |b_{D_i} (Q_{U_i} - q_i)|^{n_{D_i}}, \quad (28)$$

$$b_{D_i} = (D_{L_i} - D_{U_i})^{1/n_{D_i}} / (Q_{U_i} - Q_{L_i}), \quad (29)$$

$$n_{D_i} = \ln[D_{U_i} / (D_{U_i} - D_{L_i})] / \ln[Q_{U_i} / (Q_{U_i} - Q_{L_i})], \quad (30)$$

$$b_{B_i} = |a_{B_i}|^{1/n_{B_i}} / \Delta Q_i, \quad (31)$$

$$a_{B_i} = 1 / (1 - |Q_{O_i} / \Delta Q_i|)^{1/n_{B_i}}, \quad (32)$$

$$\Delta Q_i = (Q_{U_i} - Q_{L_i})/2, \quad (33)$$

$$Q_{O_i} = (Q_{U_i} + Q_{L_i})/2. \quad (34)$$

Yasukawa published values for the 23 parameters of the model in the original paper;<sup>24</sup> we will refer to these as the Yasu96 parameters. A revised set of parameters was pub-

lished in 2003 (Yasu03).<sup>37</sup> Both sets of parameters for Si and oxygen (O) are given in Table I, in which the parameters that are different in Yasu03 from Yasu96 are indicated by an asterisk. For Si, when there is no charge transfer and no charge for each atom, this extended potential formulation reduces to the original Tersoff potential<sup>13</sup> in both its functional form and in the values of the parameters.

## B. Tests of the Yasukawa potential

The Yasukawa<sup>24</sup> potential is a logical development of the Tersoff potentials into a COMB framework. However, since test calculations were previously only performed for the properties of  $\alpha$ -quartz ( $\alpha$ - $Q$ ), its range of validity needs to be examined further. In this section the results of a complete characterization of the Yasu96 and Yasu03 potentials for Si and five silica polymorphs are presented. Since the two versions of the potential are identical in form and only differ in the specific values of a few of the parameter, it may be presumed that the Yasu96 formalism was superseded by the Yasu03 formalism to address weaknesses or limitations in the potential identified by the original author. Nevertheless, a detailed examination of the strengths and limitations of the both parametrizations is instructive, and will guide further development. The objective of this analysis is to identify the strengths and weaknesses of the Yasukawa potentials, the extent of the range of their validity, and to help identify directions for further development and refinement.

The formation of the various polymorphs of silica involves the transfer of charge from the Si atoms to the O atoms, giving a net charge on the ions. The ability of the Yasukawa potentials to mimic this crucial effect can be assessed at two different levels. At the simpler level, it can be assumed that all of the Si ions have identical charge  $+2Q$ , while all of the O ions have identical charges of  $-Q$ , thereby maintaining the overall charge neutrality of the system (the ‘‘uniform charge’’ case). At a more physically realistic level, the charges of every individual Si and O ion can be allowed to vary individually (the ‘‘independent charge’’ case). Of course, for a spatially homogeneous system such as a crystalline phase, in the independent charge case the system should equilibrate into charge states identical to those found from the uniform charge case. In particular, as the charges are allowed to change freely, it is expected that the charge distribution for Si in the SiO<sub>2</sub> system should assume a relatively narrow distribution centered at some positive value.

### 1. Silicon

Taking Si first, we measure the lattice constant by using the Yasu96 both with and without dynamical charge transfer. For the uniform charge case, the constraint of overall charge neutrality results in all of the Si atoms carrying zero charge, in which limit Yasu96 and Yasu03 coincide with the original Tersoff potential<sup>13</sup> in functional form with the parameters. As expected, for the case of zero charge, the results for the Tersoff potential are reproduced.

For the independent charge case, the Yasu96 potential shows unphysical behavior. In particular, there is a strong

TABLE I. Potential parameters for Si and O for the 1996 and 2003 parametrizations of the Yasukawa potential, and for the COMB06 potential. The parameters that are different in Yasu03 from Yasu96 are indicated by \*. The parameters in the COMB06 potential that are different from Yasu03 are denoted in bold.

|                                 | Yasu96     |         | Yasu03     |           | COMB06        |                |
|---------------------------------|------------|---------|------------|-----------|---------------|----------------|
|                                 | Silicon    | Oxygen  | Silicon    | Oxygen    | Silicon       | Oxygen         |
| $A$ (eV)                        | 1830.81    | 3326.70 | 1830.81    | 3326.70   | 1830.81       | 3326.70        |
| $B$ (eV)                        | 471.17     | 260.89  | 471.17     | 260.89    | 471.17        | 260.89         |
| $\lambda$ ( $\text{\AA}^{-1}$ ) | 2.4799     | 5.36    | 2.4799     | 5.36      | 2.4799        | 5.36           |
| $\alpha$ ( $\text{\AA}^{-1}$ )  | 1.7322     | 2.68    | 1.7322     | 2.68      | 1.7322        | 2.68           |
| $\beta$                         | 1.0999E-06 | 2       | 1.0999E-06 | 2         | 1.0999E-06    | 2              |
| $n$                             | 0.78734    | 1       | 0.78734    | 1         | 0.78734       | 1              |
| $m$                             | 3          | 1       | 3          | 1         | 3             | 1              |
| $c$                             | 100390     | 0       | 100390     | 6.6*      | 100390        | 6.6            |
| $d$                             | 16.218     | 1       | 16.218     | 1         | 16.218        | 1              |
| $h$                             | -0.59826   | 0       | -0.59826   | -0.229*   | -0.59826      | -0.229         |
| $R_S$ ( $\text{\AA}$ )          | 2.6        | 2.6     | 2.6        | 2.6       | 2.6           | 2.6            |
| $S_S$ ( $\text{\AA}$ )          | 3          | 3       | 3          | 3         | 3             | 3              |
| $R_L$ ( $\text{\AA}$ )          | 1.1        | 1.1     | 1.1        | 1.1       | 1.1           | 1.1            |
| $S_L$ ( $\text{\AA}$ )          | 5.0        | 5.0     | 5.45*      | 5.45*     | 5.45          | 5.45           |
| $\chi$ (eV)                     | 4.375      | 7.545   | -4.85*     | 11.015*   | <b>-0.3</b>   | <b>12.006</b>  |
| $J$ (eV)                        | 7.55       | 12.13   | 5.*        | 17.71*    | <b>-4.4</b>   | <b>21.041</b>  |
| $Q_L$ ( $e$ )                   | -4         | -2      | -4         | -2        | -4            | <b>-1.8349</b> |
| $Q_U$ ( $e$ )                   | 4          | 6       | 4          | 6         | 4             | <b>5.5046</b>  |
| $D_L$ ( $\text{\AA}$ )          | 1.62       | 1.48    | 1.7982*    | 0.00148*  | 1.7982        | 0.00148        |
| $D_U$ ( $\text{\AA}$ )          | -1.54      | -1.12   | -1.7094*   | -0.00112* | -1.7094       | -0.00112       |
| $n_B$                           | 10         | 10      | 10         | 10        | 10            | 10             |
| $\eta$                          | 0.930      | 0.930   | 0.617*     | 0.419*    | 0.617         | <b>0.4567</b>  |
| $C_{VDW}$ (eV $\text{\AA}^6$ )  | 0          | 0       | 0          | 0         | 0             | 0              |
| $J_3$ (eV)                      | 0          | 0       | 0          | 0         | <b>-1.25</b>  | 0              |
| $J_4$ (eV)                      | 0          | 0       | 0          | 0         | <b>2.53</b>   | 0              |
| $q_0$ ( $e$ )                   | 0          | 0       | 0          | 0         | <b>0.6112</b> | 0              |

tendency for Si atoms to become charged, even under the constraint of total charge neutrality. This is illustrated by a simulation in which we consider a diamond-structure Si lattice as two interpenetrating Si fcc sublattices with either zero charge for all of the atoms in a single sublattice or with equal and opposite charges on the atoms in the two sublattices. As Fig. 1 shows, the zero charge for all of the atoms on each fcc sublattice is actually an energy maximum, with the energy minimum corresponding to the charges on the Si in each sublattice being +3.3 and -3.3, respectively. A similar effect was obtained for a wide range of both compressive and tensile strains. Further tests and analysis indicated that the parameter  $\eta$  (the strength of Coulombic interaction) is the dominant parameter for the formation of dipole Si formation. The corresponding test using the Yasu03, in which  $\eta$  was significantly decreased (see Table I) showed no such tendency, suggesting that this may have been one of the motivations for the development of Yasu03.

We have also characterized Si for the Yasu03 potential. For the independent charge case for Si crystal, the charge on every Si atom does not have to be exactly zero and fluctuates randomly around the charge equilibrium value zero; the

higher the temperatures the bigger the random charge fluctuation (see Fig. 2). However, these charge fluctuations are still rather small over the temperature range we studied from 0 to 1500 K. As a result of these fluctuations, while the lattice constant and cohesive energy obtained by the Yasukawa potential are exactly identical with original Tersoff potential<sup>13</sup> at zero temperature, they do not increase as rapidly with temperature as the Tersoff potential does as shown in Fig. 3. This is attributable to the presence of the small charge fluctuations; the resulting Coulombic attractions tend to increase the strength of bonding and lower the thermal expansion and energy. For comparison, the experimental results (diamonds)<sup>38</sup> and values for the Stillinger-Weber potential (open triangles)<sup>39</sup> are also shown in Fig. 3.

In the above analyses, it has been assumed that the system is overall charge neutral. In the context of building a Si/SiO<sub>2</sub> system, it is not possible to automatically guarantee that the Si will be charge neutral even if an overall charge neutrality constraint is imposed. We have therefore determined the energy and structure of Si for the uniform charge case as a function of the charge on the Si atoms. We find the unphysical result that the energy of the system is lowered by all of

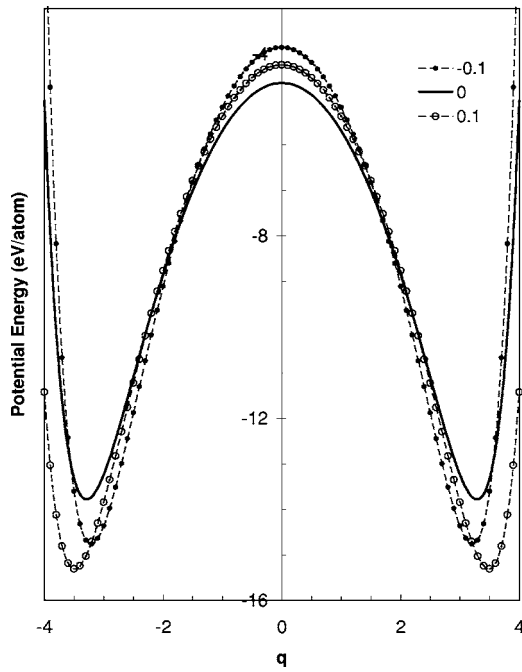


FIG. 1. Cohesive energies as a function of Si charge for interpenetrating Si fcc sublattices with equal and opposite charges at different values of isotropic strain using Yasu96 potential.

the Si atoms acquiring same positive charge as shown in Fig. 4 (circles); thus Si is keen to donate electrons to SiO<sub>2</sub>.

### 2. Silicon oxide systems

To compare with the published results for the Yasu96 potential, we first examined the case of  $\alpha$ -Q. For the uniform

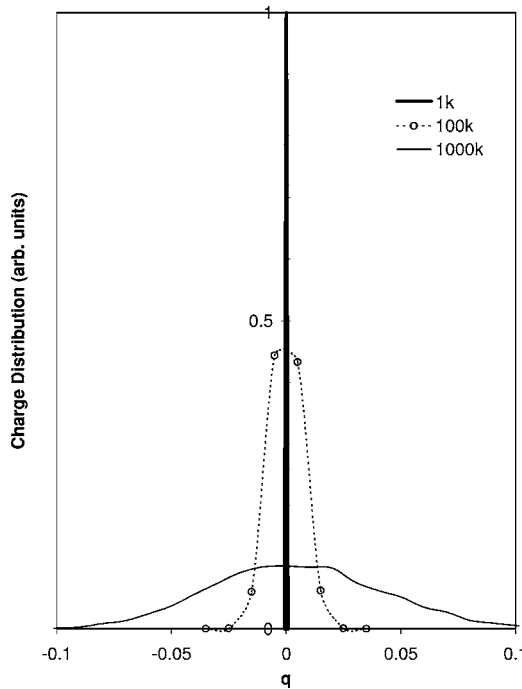


FIG. 2. The distribution of charges on Si atoms in Si as determined from the Yasukawa potential becomes broader with increasing temperature.

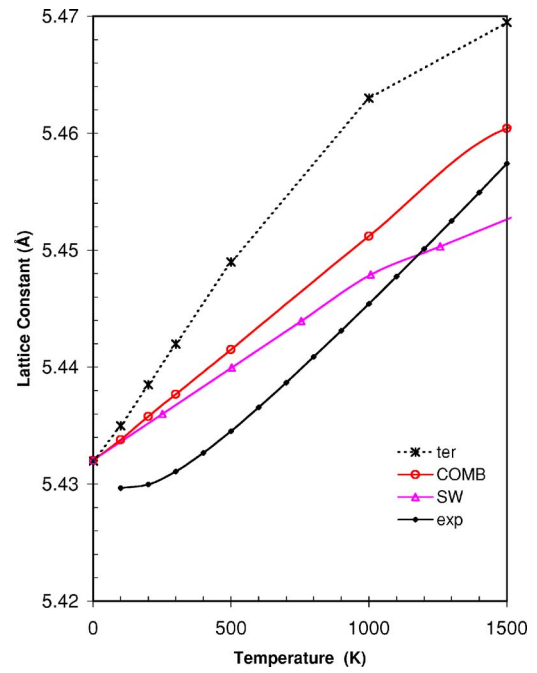


FIG. 3. (Color online) Lattice constants for silicon as a function of temperature predicted by COMB at zero pressure (open circles), as well as the values obtained by well-known Tersoff (stars) and Stillinger-Weber (open triangles) potential models, and comparing with experimental results (filled diamonds).

charge case at low temperature (e.g., 1 K), our results are consistent with the published results of Yasukawa for the lattice constant and cohesive energy. However, above room temperature (300 K), the  $\alpha$ -Q structure becomes unstable to

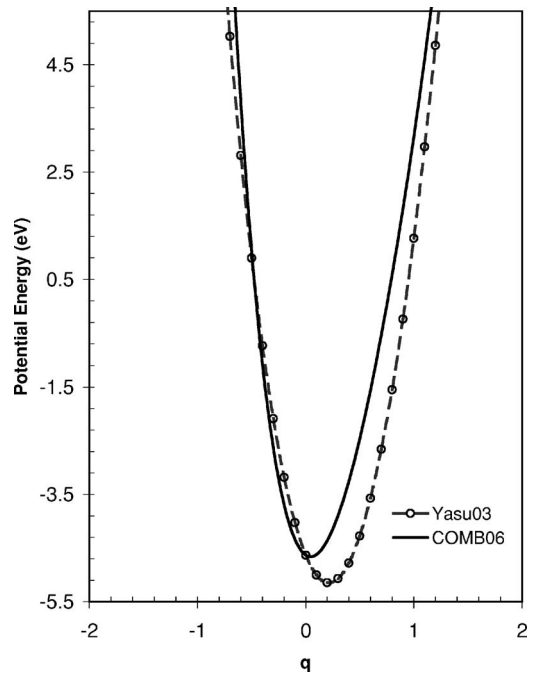


FIG. 4. The potential energies as a function Si charge by COMB06 (solid line), and comparing with Yasu03 (dashed line) for the uniform charge case.

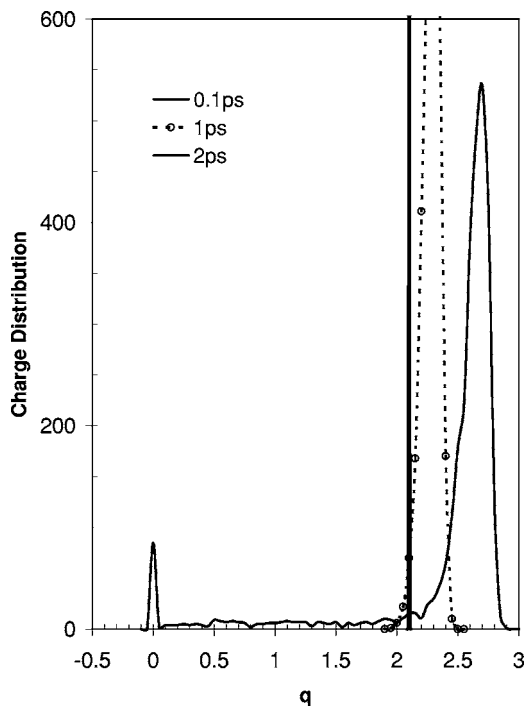


FIG. 5. The charge distribution on the Si ions in  $\alpha$ -quartz for three different times of an MD run shows the development of unphysical Si-Si charge dipoles by Yasu96.

a structure in which the bond lengths for Si-O are split into short Si-O bonds and long Si-O bonds. This is associated with a significantly lower energy state. The origin of this instability is the bond bending term, characterized by the bond angle,  $\theta_{jik}$  in Eq. (18): our tests indicate that when bond angle  $\theta_{jik}$  is treated as fixed during the force evaluation, the system is stable.

For uniform charge, the lattice constants for  $\alpha$ - $Q$  predicted by the Yasu03 potential ( $a=5.05$  Å and  $c=5.24$  Å) (Ref. 37) are significantly improved over the Yasu96 (Ref. 24) potential, as is the cohesive energy. For the uniform charge case, our results are indeed consistent with the published results of Yasukawa.<sup>37</sup>

For the independent charge case, the  $\alpha$ - $Q$  structure is unstable under both the Yasu96 and Yasu03 parametrizations. For the Yasu96 parameters, the formation of Si-Si charge dipoles, similar to those found in Si, was observed during long MD runs, as shown in Fig. 5. This is a physically unreasonable result. In order to characterize the origin of the development of these dipoles, the cohesive energies as a function of charge for the  $\alpha$ - $Q$  system with different isotropic strain were determined [see Fig. 6(a)]. As can be seen, for compressive strains (filled circles), tensile strains (open circles), and in the absence of strain, Yasu96 predicts an unphysical double energy well, with a local energy minimum for Si ions with negative charges. The charge state associated with minimum-energy configuration is shown as a function of isotropic strain in Fig. 6(b). When the  $\alpha$ - $Q$  system is under tensile strains, the Si charge prefers to be positive. However, as compressive strains are applied to the  $\alpha$ - $Q$  system, the charge for Si will be negative. In particular, for large compressive strain,  $\epsilon < -0.05$ , the global energy minimum actu-

ally has negatively charged Si ions and positively charged oxygen ions.

This spurious charge dipole effect illustrates two interesting issues. First, for any charge-transfer potential, it cannot be assumed that all atoms of the same species will have the same charge. Second, the actual charge is highly dependent on the parametrization of the potential. In fact, the corresponding tests for the Yasu03 for the  $\alpha$ - $Q$  system [Fig. 6(c)] showed no such unphysical effect, which was presumably one of the reasons for the revised parametrization for the parameter  $\eta$ .

However for the individual charge case, although the issue of the spurious Si-Si charge dipole effect is no longer present, the  $\alpha$ - $Q$  structure is still unstable under the Yasu03 parametrizations. In particular, the charge distribution for Si in SiO<sub>2</sub> is still not Gaussian centered at some positive value by Yasu03, as shown in Fig. 7 and the bond lengths for Si-O are split. Again, this instability is induced by the term of bond angle  $\theta_{jik}$  in Eq. (18). Finally, for the uniform charge case we determined the Si and O charge that yielded the lowest total energy for the system.

In the above analyses, it has been assumed that the system is overall charge neutral. As noted before, in the context of building a Si/SiO<sub>2</sub> system, it is not possible to automatically guarantee that the SiO<sub>2</sub> will be charge neutral even if an overall charge neutrality constraint is imposed. We have therefore determined the energy of SiO<sub>2</sub> for the uniform charge case as a function of the charge on the Si and O atoms. The results for  $\alpha$ - $Q$  are shown in Fig. 8 in which the horizontal axis represents O charge, and vertical axis Si charge. For reference, the diagonal line corresponds to charge neutrality for which the O/Si charge ratio is  $-1/2$ . As can be seen, the minimum potential energy for  $\alpha$ - $Q$  is not located on the reference red line. Very similar results are obtained for other structures. In particular, the energy minimum as for charges for Si of 1.68 and  $-0.9$  for O, the system is not charge neutral. As a result, silica strongly prefers to accept some electrons if electrons are available. However, this does not happen for the pure silica system since it is isolated and charge neutrality is guaranteed. On the other hand, as discussed above, Si is ready to donate electrons. It is not surprising therefore that as we will see below, when Si contacts with SiO<sub>2</sub>, the issue of charge transfer from Si to SiO<sub>2</sub> is important.

Despite the limitations of the potential we were able to determine the structure and energy of various SiO<sub>2</sub> polymorphs using Yasu03 for the independent charge case. The results of cohesive energy for five different silica polymorphs are listed in Table II and compared with experimental results.<sup>40,41</sup> For comparison, the results from the fixed charge TTAM potential<sup>42</sup> and the ReaxFF potential are also given in Table II. As can be seen Yasu03 predicts a value for the cohesive energy for  $\alpha$ - $Q$  that is very close to the experimental value. However, the order of the stability of the silica polymorphs predicted by Yasu03 does not agree with experiment. In particular,  $\alpha$ - $Q$  is not predicted to be the most stable phase of silica. Of particular concern is the poor agreement for both  $\alpha$ - and  $\beta$ -cristobalite ( $\alpha$ - $C$  and  $\beta$ - $C$ ) which are caused by the formation of unphysical linear O-Si-O units. Interestingly, the TTAM fixed charge potential can accurately

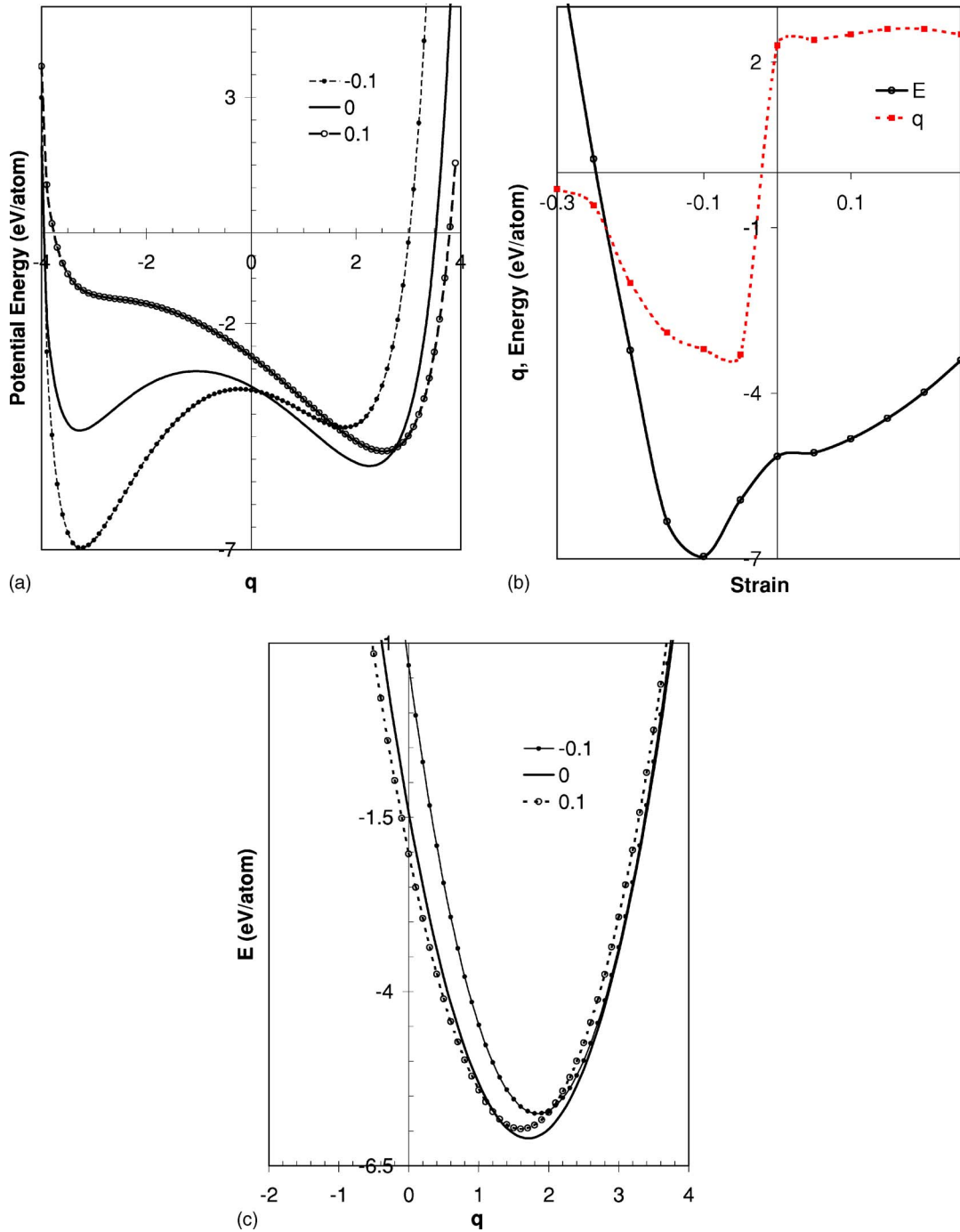


FIG. 6. (Color online) (a) Cohesive energies as a function of Si charge for  $\alpha$ -quartz system (solid lines), as well as isotropic compressive strain (filled circles) and tensile strain (open circles) by Yasu96; (b) Minimum energies (open circles) and corresponding Si charges (filled squares) as a function of isotropic strain by Yasu96. (c) Cohesive energies as a function of Si charge for  $\alpha$ -quartz system (solid lines), as well as isotropic compressive strain (filled circles) and tensile strain (open circles) by Yasu03.

reproduce  $\alpha$ - $Q$  as the most stable structure, but the cohesive energy for  $\alpha$ - $Q$  was predicted to be about  $-7.4$  eV per atom,<sup>42</sup> a rather large difference from the experimental energy ( $-6.41$  eV/atom) (Ref. 40). Moreover, the order in energy of  $\beta$ - $Q$  and  $\alpha$ - $C$  is reversed relative to the experimental values. Finally, although the ReaxFF (Ref. 26) potential correctly predicted the relative energies of  $\alpha$ - $C$  and  $\alpha$ - $Q$ , it also incorrectly predicted  $\beta$ -tridymite ( $\beta$ - $T$ ) to have a lower energy than either.

#### IV. COMB06 POTENTIAL FOR Si AND SiO<sub>2</sub>

Although the extended Tersoff potential by Yasukawa<sup>24</sup> makes significant progress towards achieving many-body interaction with dynamical charge transfer for MD simulations of the Si-SiO<sub>2</sub> system, as discussed above our test results revealed that it still has a number of flaws. In this section, we describe modifications to the Yasu03 potential that resolve these issues. We dub this new potential the COMB06 poten-

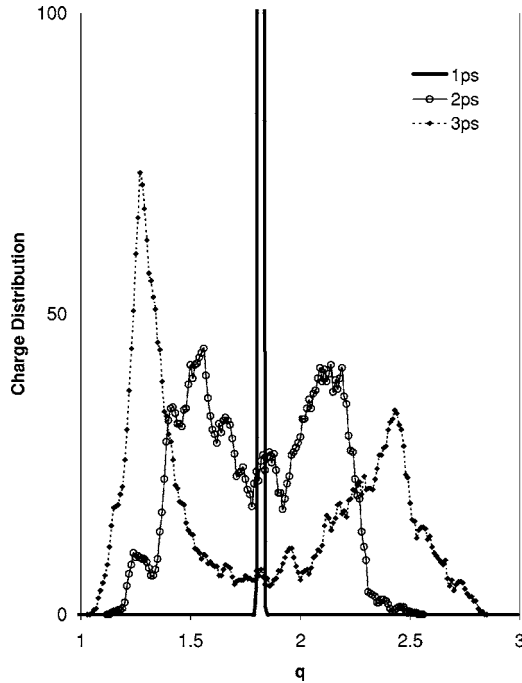


FIG. 7. The charge distribution on the Si ions in  $\alpha$ -quartz for three different times of an MD run shows the charge divergence by Yasu03.

tial for Si and  $\text{SiO}_2$ . Our objective is to develop a potential that has all of the positive attributes of the Yasukawa, while in addition giving

- (i) charge neutrality as the lowest energy states for both Si and  $\text{SiO}_2$ ;
- (ii) the correct relative stabilities of the polymorphs of  $\text{SiO}_2$ , and lattice constants close to experimental values;
- (iii) a unimodal distribution for the Si-O bond lengths;
- (iv) correct bond angles in the  $\text{SiO}_2$  polymorphs.

In the following sections, we systematically outline how to build these attributes into the potential.

### A. Local charge neutrality

In the simulations of either pure Si or pure  $\text{SiO}_2$  we have taken the simulation cell to be charge neutral. However, for a system that contains both Si and  $\text{SiO}_2$ , such as a heterogeneous interface, the individual components cannot be held charge neutral, but only the charge on the simulation cell as a whole. It is thus important to determine the charge states of Si and  $\text{SiO}_2$  at the energy minimum. In the previous analyses of the Yasukawa potential, it was found that as Si contacts with  $\text{SiO}_2$ , silica strongly prefers to accept charge and Si readily donates charge, which leads to a non-neutral background charge for both the Si and the  $\text{SiO}_2$  layers, as illustrated in Fig. 9 (dashed lines).

In order to better ensure charge neutrality for both the Si and  $\text{SiO}_2$  systems, further modifications of the self-energy term are necessary. In particular, the modification we adopt is based on the consideration that it should affect the properties of bulk silicon and bulk silica as little as possible, and it

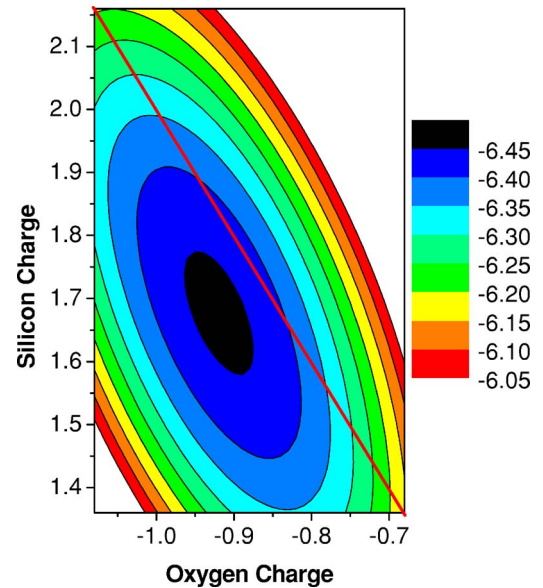


FIG. 8. (Color online) The potential energies as a function in the charge space for  $\alpha$ - $Q$ . Horizontal axis is the charge for oxygen and vertical for silicon by Yasu03.

should be continuous and smooth to avoid spurious jumps in either the particle or charge forces. We modify the self-energy term in Eq. (1) to

$$E_i^S(q_i) = \chi_i(q_i - q_0) + \frac{1}{2}J_i(q_i - q_0)^2 + J_{3-i}(q_i - q_0)^3 + J_{4-i}(q_i - q_0)^4. \quad (35)$$

In fact, this modification does not affect the self-energy for O, i.e.,  $J_3 = J_4 = q_0 = 0$ . For Si, we have determined a suitable set of parameters to be  $\chi = -0.3$  eV,  $J = -4.4$  eV,  $J_3 = -1.25$  eV,  $J_4 = 2.53$  eV, and  $q_0 = 0.6112$ , as listed in Table I. The resulting potential energy as a function of Si charge for a Si crystal by the COMB06 potential is shown in Fig. 4 (solid line). The corresponding charge for the minimum energy of the Si crystal is very nearly neutral ( $q_{\text{Si}} = 0.001$ ), a

TABLE II. Cohesive energies for  $\alpha$ -quartz (in units of eV/atom) and energies relative to  $\alpha$ -quartz for four other silica polymorphs. The Yasu03 potential gives the incorrect order of energies and particularly poor agreement for both  $\alpha$ - and  $\beta$ -cristobalite. The COMB06 potential predicts the correct order of stability for the different phases.  $Q$ =quartz,  $C$ =cristobalite,  $T$ =tridymite.

|                | Symmetry | Expt. <sup>a</sup> | Yasu03 | TTAM <sup>b</sup> | ReaxFF <sup>c</sup> | COMB06 |
|----------------|----------|--------------------|--------|-------------------|---------------------|--------|
| $\alpha$ - $Q$ | Tri.     | -6.410             | -6.425 | -7.4              |                     | -6.444 |
| $\alpha$ - $C$ | Ter.     | +0.010             | -0.955 | +0.062            | +0.001              | +0.003 |
| $\beta$ - $Q$  | Hex.     | +0.017             | -0.001 | +0.021            |                     | +0.006 |
| $\beta$ - $C$  | Cubic    | +0.018             | -0.255 | +0.071            |                     | +0.067 |
| $\beta$ - $T$  | Hex.     |                    | 0      | +0.086            | -0.005              | +0.05  |

<sup>a</sup>References 40 and 41.

<sup>b</sup>Reference 42.

<sup>c</sup>Reference 26.

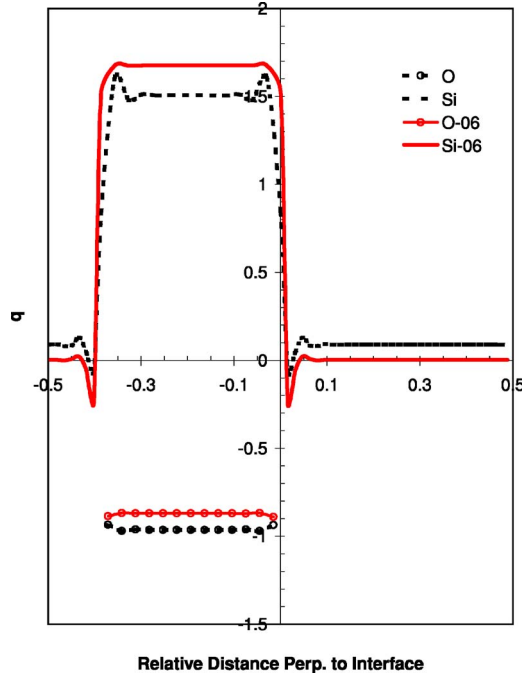


FIG. 9. (Color online) The charge distribution of Si/ $\beta$ -C interface for both Si and O (open symbols) along  $x$  axis with local charge correction terms (solid lines), as well as without charge correction terms (dashed lines) by COMB06 potential.

significant improvement over the Yasu03 potential ( $q_{\text{Si}}=0.2$ ). Meanwhile, in order to make the minimum potential energy for  $\text{SiO}_2$  systems satisfy the requirement of charge neutrality without introducing appreciable change in the structure, five parameters related to charge for O were re-optimized and are also listed in Table I; in Table I parameters in the COMB06 potential that are different from Yasu03 are denoted in bold.

The result for charge distribution at the Si/ $\beta$ -C interface for both Si and O (circles) along the  $z$  axis is shown in Fig. 9 with charge correction terms (solid lines), as well as without charge correction terms (dash lines). The results indicate that the issue of non-neutrality in the Si and  $\text{SiO}_2$  is significantly improved. It is also worthwhile to note that this type of background charge is also present for the Al/ $\text{Al}_2\text{O}_3$  system<sup>43</sup> described using the Streitz-Mintmire potential,<sup>28</sup> and is possibly a common issue for charge-transfer potentials. We conclude that to develop a physically reasonable charge-transfer potential, the global minimum potential energy for each of the pertinent material systems should be charge neutral. In the case of Si and  $\text{SiO}_2$  systems, in order to obtain the minimum potential energy, the charge for bulk Si should be zero in charge space and the charge ratio of Si/O for silica should be  $-1/2$ .

### B. Bond-bending terms

As described in Sec. 3.2.3 (iv) above, in Yasu03, linear O-Si-O units are formed in  $\alpha$ -C, a structure that is not physically correct. The problem is exemplified by an isolated O-Si-O monomer which when relaxed with Yasu03 always

forms a linear  $\text{SiO}_2$  structure. To fix this problem, we introduce a bond-bending term as the bond angle between  $ij$  and  $ik$  in O-Si-O to the total potential-energy function  $E_T$  of the form

$$E_{\text{OSiO}} = \sum_i \sum_{j \neq i} \sum_{k \neq i, j} f_{C_{ij}} f_{C_{ik}} K_{\text{OSiO}} (\cos \theta_{\text{OSiO}} - \cos \theta_{\text{OSiO}}^0)^2. \quad (36)$$

The cutoff function  $f_C$  is defined by Eq. (21) in which  $R_{\text{SiO}}=2.6 \text{ \AA}$  and  $S_{\text{SiO}}=3.0 \text{ \AA}$ . The choice of  $K_{\text{OSiO}}=9.5 \text{ eV}$  and  $\theta_{\text{OSiO}}^0=109.47^\circ$  (the ideal tetrahedral bond angle) gives a  $\text{SiO}_2$  monomer with bond angle  $\theta_{\text{OSiO}}^0=109.47^\circ$  to be the most stable structure. The addition of this term to the potentials results in the eliminations of the linear O-Si-O units in  $\alpha$ -C. Furthermore, the charge distribution for Si in all silicon oxide polymorphs is significantly converged to a Gaussian distribution, and the bond lengths distribution for Si-O is unimodal.

While the above modification results in  $\alpha$ -C and  $\beta$ -C structures that are structurally consistent with experiment, it still predicts that  $\alpha$ -C is the most stable  $\text{SiO}_2$  phase. Moreover, it does not give correct lattice parameters for the five polymorphs. To address these issues, i.e., (ii) and (iii) above, an additional energy term was introduced as the bond angle between  $ij$  and  $ik$  in Si-O-Si,

$$E_{\text{SiOSi}} = \sum_i \sum_{j \neq i} \sum_{k \neq i, j} f_{C_{ij}} f_{C_{ik}} K_{\text{SiOSi}} (\cos \theta_{\text{SiOSi}} - \cos \theta_{\text{SiOSi}}^0)^2, \quad (37)$$

in which  $K_{\text{SiOSi}}=4.5 \text{ eV}$  is optimized to bond angle  $\theta_{\text{SiOSi}}^0=143.73^\circ$ . This additional term has the desired effect of making the  $\alpha$ -Q system the most stable polymorph. After adding this energy penalty term to the total potential-energy function, the lattice constants along the  $c$  axis are significantly improved for all five silica polymorphs and the stability order of silica polymorphs predicted by COMB06 is agreement with experimental results.

### C. Correcting the cohesive energies

As the bond length of Si-O decreases, the repulsive energy term [Eq. (12)] weakens and thus leads to a short lattice constant along the  $c$  axis for the silica polymorphs. The charge neutrality correction leads to an increase in the cohesive energy. In order to bring the cohesive energy and lattice constants closer to experimental values, an additional repulsive term, shown in the square brackets, is introduced to Eq. (12):

$$U_{ij}^R(r_{ij}, q_i, q_j) = f_{S_{ij}} A_{ij} e^{(-\lambda_{ij} r_{ij})} [1 + K_r (1 - r_{ij}/r_{ij}^0)^2]. \quad (38)$$

Here  $K_r=20 \text{ eV}$  and  $r_{ij}^0=1.65 \text{ \AA}$  are applied only to Si-O bonds. These extensions to the original Yasu03 potential result in good agreement for the  $\text{SiO}_2$  polymorph energies and structures and, importantly, have no effect on Si.

### D. Evaluation of COMB06 for silicon and silicon oxide

The COMB06 potential, defined by the above modifications to the Yasu03 potential and by the parameters given in

TABLE III. Lattice constants ( $\text{\AA}$ ) of silica polymorphs using the COMB06 potential, compared with the TTAM potential and experiment. The parameters in the COMB06 potential that are better than TTAM potential are denoted in bold.

|                     | COMB06   |              |              | TTAM <sup>a</sup> |          | Expt.              |                    |
|---------------------|----------|--------------|--------------|-------------------|----------|--------------------|--------------------|
|                     | <i>q</i> | <i>a</i>     | <i>c</i>     | <i>a</i>          | <i>c</i> | <i>a</i>           | <i>c</i>           |
| $\alpha$ - <i>Q</i> | 1.70     | <b>4.996</b> | <b>5.325</b> | 5.02              | 5.53     | 4.916 <sup>b</sup> | 5.405 <sup>b</sup> |
| $\alpha$ - <i>C</i> | 1.70     | 4.942        | 6.286        | 4.96              | 6.68     | 4.96 <sup>c</sup>  | 6.89 <sup>c</sup>  |
| $\beta$ - <i>Q</i>  | 1.69     | <b>5.008</b> | <b>5.332</b> | 5.17              | 5.73     | 5.01 <sup>d</sup>  | 5.47 <sup>d</sup>  |
| $\beta$ - <i>C</i>  | 1.69     | 7.014        |              | 7.07              |          | 7.16 <sup>e</sup>  |                    |
| $\beta$ - <i>T</i>  | 1.70     | <b>4.985</b> | <b>8.156</b> | 5.37              | 8.75     | 5.03 <sup>f</sup>  | 8.22 <sup>f</sup>  |

<sup>a</sup>Reference 42.

<sup>b</sup>Reference 44.

<sup>c</sup>Reference 45.

<sup>d</sup>References 46 and 47.

<sup>e</sup>References 46 and 48.

<sup>f</sup>References 46 and 49.

Table I, gives results for Si that are identical to the Yasukawa potentials since the functional form and parameters are the same. In addition, the COMB06 potential predicts the correct energy order for the silica polymorphs as shown in Table II. In particular, the cohesive energies are in good overall agreement with the experimental values, although the difference between the energies of  $\beta$ -*C* and  $\beta$ -*Q* is significantly larger than the experimental difference. Moreover, the lattice constants predicted by the COMB06 potential for Si and SiO<sub>2</sub> are significantly improved for  $\alpha$ -*Q*, as indicated in Table III. Furthermore, the lattice constants for the other four silica polymorphs also compare reasonably well with experimental values<sup>44-49</sup> as presented in Table III. In order to minimize finite-size effects, a system size consisting of at least ten conventional unit cells in three dimensions is used with periodic boundary conditions. The optimization of the atomic geometry of all the silica polymorphs is performed via the minimization of the total energy with respect to the lattice constants and atomic coordinates. In spite of the satisfying results for silica polymorphs, the performance of the COMB06 potential for amorphous silica is disappointing, with preliminary results indicating that quenched amorphous silica transforms spontaneously into a crystal phase.

The average charge for Si in the various silica polymorphs is presented in Table III. The equilibrium charge for Si in each silicon oxide structure is almost identical and the Gaussian charge distribution is centered at +1.7, which indicates that charge distribution is not very sensitive to the structure. Since the Si-O bond is a mixture of partially ionic and partially covalent bond types, the fractional charges used in the COMB06 potential represent an incomplete charge transfer between the ions. We note that in fixed charge potentials such as TTAM (Ref. 21) and BKS (Ref. 22) the silicon and oxygen ions have charges of +2.4 and O -1.2, respectively, and these charge values are higher than in the COMB06 potential. Interestingly the more complex ReaxFF SiO potential<sup>26</sup> assigns charges of +1.346 to Si and -0.673 to O atoms in  $\alpha$ -quartz, which are lower than the values used in COMB06.

To summarize, the cohesive energy and lattice constants for five silica polymorphs predicted by COMB06 have been presented at 1 K and compared with experimental data and values predicted by other well-known potentials. The following sections now present additional structural properties of the various silica polymorphs, such as bond lengths and bond angles, as predicted by COMB06.

### 1. $\alpha$ -quartz

The COMB potential predicts the equilibrium volume per SiO<sub>2</sub> unit of  $\alpha$ -*Q* to be 38.37  $\text{\AA}^3$ , which is less than 1.8% larger than the experimental value.<sup>44</sup> Corresponding to this overestimated volume, the bond lengths are 1.638 and 1.636  $\text{\AA}$ , which are longer than the experimental values of 1.614 and 1.605  $\text{\AA}$ .<sup>44</sup> The corresponding O-Si-O bond angles are 109.57°, 109.82°, 109.65°, and 108.98°, which compare well with the measured experimental data of 109.0°, 110.5°, 109.2°, and 108.8°.<sup>44</sup> The Si-O-Si bond angle of 140.4° shows a somewhat large deviation from the experiment value of 143.7°,<sup>44</sup> and leads to a shorter *c* axis. This is most likely caused by the relatively weak correction for the Si-O-Si bond angle.

### 2. $\alpha$ -cristobalite

The volume of  $\alpha$ -*C* is predicted to be 38.37  $\text{\AA}^3$ , which underestimates the equilibrium volume by as much as 10.3%, compared with 42.77  $\text{\AA}^3$  obtained from experiment at 10 K.<sup>45</sup> Despite the too-small volume, the Si-O bond lengths are 1.6334 and 1.6288  $\text{\AA}$ , which are longer than the experimental results of 1.6026 and 1.6034  $\text{\AA}$ .<sup>45</sup> The compression of the volume influences the Si-O-Si bond angle, determined to be 135.3°, much more than the bond length, and this leads to a significant deviation from experimental value of 146.5°. This lower Si-O-Si bond angle may explain the shorter *c* axis predicted for  $\alpha$ -*C*. The predicted O-Si-O bond angles are 109.3°, 110.1°, 109.8°, and 108.3° which are quite consistent with the experimental values of 109.0°, 111.4°, 110.0°, and 108.2°.<sup>45</sup>

### 3. $\beta$ -quartz

The volume of  $\beta$ -*Q* is predicted to be 38.52  $\text{\AA}^3$ , which underestimates the equilibrium volume by 2.2%.<sup>46,47</sup> Despite the small volume, the Si-O bond lengths range from 1.625 to 1.641  $\text{\AA}$ , and are significantly longer than the experimental value of 1.5895  $\text{\AA}$ .<sup>46,47</sup> This discrepancy is probably caused by the Si-O bond length penalty. Since the O-Si-O bond angles of 110.1°, 109.8°, and 108.5° are consistent with the experimental values of 111.3°, 110.1°, and 107.0°,<sup>46,47</sup> in order to maintain the volume of the crystal the Si-O-Si bond angle deviates significantly from the experimental value of 153.0°, and ranges from 134.0° to 151.0°. These lower Si-O-Si bond angles explain the shorter *c* axis predicted for  $\alpha$ -*C*.

### 4. $\beta$ -cristobalite

The volume of  $\beta$ -*C* is predicted to be 43.00  $\text{\AA}^3$ , which is 5.1% lower than the 45.33  $\text{\AA}^3$  obtained from experiment.<sup>45</sup> Despite the smaller volume, the Si-O bond lengths are be-

tween 1.62 and 1.64 Å, which are on average 0.02 Å longer than experimental result of 1.61 Å.<sup>46,48</sup> The O-Si-O bond angles are between 107.7° and 111.4°, which are also consistent with the experimental values of 107.8° and 112.9°. Thus the compression of the volume influences the Si-O-Si bond angle much more than the bond length and leads to a significant deviation from experimental values (predicted values are 133.0° and 159.0° and experimental values are 137.2° and 180.0°).

### 5. $\beta$ -tridymite

COMB06 predicts a quite accurate equilibrium volume of 43.69 Å<sup>3</sup> for this polymorph, which underestimates the equilibrium volume by 3.1% compared with 45.11 Å<sup>3</sup> obtained from experiment.<sup>46,49</sup> However, the calculated Si-O bond lengths are between 1.62 and 1.64 Å, which are on average about 0.08 Å larger than the experimental values. The larger Si-O distances are compensated by a larger deviation of the Si-O-Si bond angles from the idealized value of 180°. Similar behavior was also predicted in DFT calculations.<sup>7</sup>

## V. Si/SiO<sub>2</sub> INTERFACE

Due to its unique properties, the structure of the Si-SiO<sub>2</sub> interface has a critical effect on the performance of silicon MOS/CMOS devices. Experiments reveal complex behavior for oxide-silicon interfaces, and atomic scale methods such as DFT have proved to be crucial in developing deeper insight into this system. It should be noted, however, that structural models used in DFT calculations rely heavily on empirical information, even in the case of the apparently simplest interfacial case of SiO<sub>2</sub>/Si(100). In particular, in order to reproduce the characteristics observed in selected experiments, DFT structural models are constructed by removing oxygen atoms and adjusting the oxygen deficiency to capture the presence of a substoichiometric oxide and its features.<sup>50-52</sup> Furthermore, due to the small number of atoms in the DFT supercells, it is difficult to avoid the creation of unrealistic mechanical forces and/or electric polarization.

A more flexible, variable charge, empirical scheme, such as COMB06, is needed to complement electronic structure calculations and experimental measurements and predict how the interface may be affected by changes in the physical conditions and/or by chemical modification of the interface. Here, the COMB06 potential is applied to study the Si(100)/SiO<sub>2</sub> interface. In order to construct a structural transition without coordination defects between the substrate and the oxide in the Si(100)-SiO<sub>2</sub> model interfaces considered here, we match pseudomorphically ideal  $\beta$ -C to Si(100) and assume an atomically abrupt interface between them.

The interfacial system is periodic, contains 15 600 atoms, and consists of a Si slab made up of an arrangement of 10 × 10 × 10 conventional unit cells and a silica slab made up of 3 × 10 × 10 conventional unit cells of  $\beta$ -C. The Si lattice parameter is chosen to be equal to 5.43 Å, which corresponds to the relaxed lattice constant of bulk Si predicted in our theoretical framework. With respect to the in-plane orientation, SiO<sub>2</sub>(010) is arranged parallel to Si(010), and

SiO<sub>2</sub>(001) is arranged parallel to Si(001). As a result, the in-plane lattice constant of SiO<sub>2</sub> contracts by 22.9% along both the [010] and [001] directions. The lattice constant of the superlattice along the  $x$  axis parallel to the [100] direction (i.e., along the modulation direction) is determined to minimize the total energy. All the atomic positions and charges in the supercell are also optimized.

We note that this model interface is highly artificial. However, the choice of  $\beta$ -C is motivated by several factors. First, this SiO<sub>2</sub> polymorph allows us to build a Si-SiO<sub>2</sub>-Si superlattice with equivalent Si-SiO<sub>2</sub> and SiO<sub>2</sub>-Si interfaces. In this way, dipolar effects arising from asymmetric interface structures are avoided. Second, it is a good example to examine the validity of our framework since the interface is highly strained.

The results for charge distribution (solid lines) for both Si and O (open circles) along the  $x$  axis after 100 ps of MD simulation with dynamic charge transfer at 1 K are shown in Fig. 9. The capability of dynamic charge transfer as an intrinsic feature of the COMB potential function allows the properties of the substoichiometric oxide in the interfacial layers to be captured automatically. A similar charge distribution is also obtained for Si/ $\beta$ -C at 700 K. However, at 700 K the abrupt interface is significantly distorted relative to the interface at 1 K. This may be explained by the stress energy induced by the difference in the thermal expansions of the Si and SiO<sub>2</sub>.

Within the frame of dynamic charge transfer, the charge distribution for Si fluctuates around the equilibrium value in a very small range for both bulk Si and silica. At the Si/SiO<sub>2</sub> interface itself, we expect a reduced charge on the Si in the first Si layer. Moreover, the charge distribution close to the Si-SiO<sub>2</sub> interface should decrease smoothly and monotonically with increasing distance from the interface. However, an unanticipated effect is observed, where the charge distribution for silicon layers near the interface oscillates significantly and decreases nonmonotonically over several Si layers to finally reach a neutral value (Fig. 9). This is most likely due to the fact that we electrostatically created an electrical double layer that reduces Coulombic repulsion interaction and thus forms multiple, pseudodipole Si layers (“charge mirror”) near the Si/SiO<sub>2</sub> interface.

## VI. CONCLUSIONS

In conclusion, a framework is developed in which Si/SiO<sub>2</sub> systems can be investigated using massively parallel molecular-dynamics simulations. Such a tool will allow for the simulation of real, nanosized devices. In order to investigate dynamic processes and interfacial properties, a new COMB potential, based on the extended Tersoff and Yakusawa potentials, is proposed and implemented in which both the effects of charge-transfer and many-body interactions are taken into account. The validity of the potential function is tested for both Si and multiple silica systems. The structural properties for Si and various polymorphs of silica are predicted to agree well with experimental results. Moreover, with the capability of dynamic charge transfer as an intrinsic feature of the potential function, important features

such as substoichiometric oxide formation around the interface between silicon and silicon oxides are captured automatically.

We have proposed an important criterion for a physically reasonable potential with charge transfer here, i.e., the global minimum potential energy should be minimized for the charge neutral state of all the pertinent phases. With an appropriate parametrization of the COMB06 potential we find that charges on the Si and O ions in the polymorphs of SiO<sub>2</sub> are similar. Indeed, we find that a fixed charge potential,

based on the COMB, well reproduces the structure and energetics of all the silica polymorphs.<sup>53</sup>

#### ACKNOWLEDGMENTS

We gratefully acknowledge many valuable conversations with Julian Gale, Alan McGaughey, and Inkook Jang. We also gratefully acknowledge the financial support of the National Science Foundation under Grant No. DMR-0426870.

- <sup>1</sup>M. Schulz, *Nature (London)* **399**, 729 (1999).
- <sup>2</sup>C. R. Helms and B. E. Deal, *The Physics and Chemistry of SiO<sub>2</sub> and the Si-SiO<sub>2</sub> Interface 2* (Plenum, New York, 1993).
- <sup>3</sup>G. Moore, *Electronics* **38**, 114 (1965).
- <sup>4</sup>R. McWeeny, *Methods of Molecular Quantum Mechanics* (Academic, New York, 1989).
- <sup>5</sup>P. Hohenberg and W. Kohn, *Phys. Rev.* **136**, B864 (1964).
- <sup>6</sup>W. Kohn and L. J. Sham, *Phys. Rev.* **140**, A1133 (1965).
- <sup>7</sup>T. Demuth, Y. Jeanvoine, J. Hafner, and J. G. Angyan, *J. Phys.: Condens. Matter* **11**, 3833 (1999).
- <sup>8</sup>A. Korkin, J. C. Greer, G. Bersuker, V. V. Karasiev, and R. J. Bartlett, *Phys. Rev. B* **73**, 165312 (2006).
- <sup>9</sup>R. Car and M. Parrinello, *Phys. Rev. Lett.* **55**, 2471 (1985).
- <sup>10</sup>M. C. Payne, M. P. Teter, D. C. Allan, T. A. Arias, and J. D. Joannopoulos, *Rev. Mod. Phys.* **64**, 1045 (1992).
- <sup>11</sup>F. H. Stillinger and T. A. Weber, *Phys. Rev. B* **31**, 5262 (1985).
- <sup>12</sup>R. Biswas and D. R. Hamann, *Phys. Rev. B* **36**, 6434 (1987).
- <sup>13</sup>J. Tersoff, *Phys. Rev. B* **38**, 9902 (1988).
- <sup>14</sup>J. Tersoff, *Phys. Rev. B* **37**, 6991 (1988).
- <sup>15</sup>J. Tersoff, *Phys. Rev. B* **39**, 5566 (1989).
- <sup>16</sup>M. Z. Bazant and E. Kaxiras, *Phys. Rev. B* **56**, 8542 (1997).
- <sup>17</sup>X. P. Li, G. Chen, P. B. Allen, and J. Q. Broughton, *Phys. Rev. B* **38**, 3331 (1988).
- <sup>18</sup>L. J. Porter, S. Yip, M. Yamaguchi, H. Kaburaki, and J. M. Tang, *J. Appl. Phys.* **81**, 96 (1997).
- <sup>19</sup>D. Srivastava and B. J. Garrison, *J. Chem. Phys.* **95**, 6885 (1991).
- <sup>20</sup>D. Srivastava and B. J. Garrison, *Phys. Rev. B* **47**, 4464 (1993).
- <sup>21</sup>S. Tsuneyuki, M. Tsukada, H. Aoki, and Y. Matsui, *Phys. Rev. Lett.* **61**, 869 (1988).
- <sup>22</sup>B. W. H. v. Beest, G. J. Kramer, and R. A. v. Santen, *Phys. Rev. Lett.* **64**, 1955 (1990).
- <sup>23</sup>T. Watanabe, H. Fujiwara, H. Noguchi, T. Hoshino, and I. Ohdomari, *Jpn. J. Appl. Phys., Part 2* **38**, L366 (1999).
- <sup>24</sup>A. Yasukawa, *JSME Int. J., Ser. A* **39**, 313 (1996).
- <sup>25</sup>S. R. Billeter, A. Curioni, D. Fischer, and W. Andreoni, *Phys. Rev. B* **73**, 155329 (2006).
- <sup>26</sup>A. C. T. v. Duin, A. Strachan, S. Stewman, Q. Zhang, X. Xu, and I. William A. Goddard, *J. Phys. Chem. A* **107**, 3803 (2003).
- <sup>27</sup>A. K. Rappe and W. A. Goddard III, *J. Phys. Chem.* **95**, 3358 (1991).
- <sup>28</sup>F. H. Streitz and J. W. Mintmire, *Phys. Rev. B* **50**, 11996 (1994).
- <sup>29</sup>D. W. Brenner, *Phys. Rev. Lett.* **63**, 1022 (1989).
- <sup>30</sup>T. Iwasaki and H. Miura, *J. Mater. Res.* **16**, 1789 (2001).
- <sup>31</sup>S. Izvekov, M. Parrinello, C. J. Burnham, and G. A. Voth, *J. Chem. Phys.* **120**, 10896 (2004).
- <sup>32</sup>S. Nosé, *J. Chem. Phys.* **81**, 511 (1984).
- <sup>33</sup>S. W. Rick, S. J. Stuart, and B. J. Berne, *J. Chem. Phys.* **101**, 6141 (1994).
- <sup>34</sup>H. Goldstein, *Classical Mechanics* (Addison-Wesley, Reading, MA, 1980).
- <sup>35</sup>M. P. Allen and D. J. Tildesley, *Computer Simulation of Liquids* (Clarendon, Oxford, 1987).
- <sup>36</sup>D. J. Keffer and J. W. Mintmire, *Int. J. Quantum Chem.* **80**, 733 (2000).
- <sup>37</sup>A. Yasukawa, in *Japan Society of Mechanical Engineers* (Hitachi City, Ibaraki, Japan, Sept. 19, 2003), p. 71.
- <sup>38</sup>Y. Okada and Y. Tokumaru, *J. Appl. Phys.* **56**, 314 (1984).
- <sup>39</sup>S. J. Cook and P. Clancy, *Phys. Rev. B* **47**, 7686 (1993).
- <sup>40</sup>P. Richet, Y. Bottinga, L. Denielou, J. P. Petitet, and C. Tequi, *Gochim. Cosmochim. Acta* **46**, 2639 (1982).
- <sup>41</sup>*CRC Handbook of Chemistry and Physics*, 64th ed. (CRC, Boca Raton, FL, 1983).
- <sup>42</sup>N. R. Keskar and J. R. Chelikowsky, *Phys. Rev. B* **46**, 1 (1992).
- <sup>43</sup>A. J. H. McGaughey, B. Devine, S. Phillpot, and S. Sinnott (unpublished).
- <sup>44</sup>L. Levien, C. T. Prewitt, and D. J. Weidner, *Am. Mineral.* **65**, 920 (1980).
- <sup>45</sup>J. J. Pluth, J. V. Smith, and J. Faber, *J. Appl. Phys.* **57**, 1045 (1985).
- <sup>46</sup>R. W. G. Wyckoff, *Crystal Structures*, 4th ed. (Interscience, New York, 1974).
- <sup>47</sup>A. F. Wright and M. S. Lehmann, *J. Solid State Chem.* **36**, 371 (1981).
- <sup>48</sup>A. F. Wright and A. J. Leadbetter, *Philos. Mag.* **31**, 1391 (1975).
- <sup>49</sup>K. Kihara, *Z. Kristallogr.* **148**, 237 (1978).
- <sup>50</sup>A. Pasquarello, M. S. Hybertsen, and R. Car, *Phys. Rev. B* **53**, 10942 (1996).
- <sup>51</sup>R. Buczko, S. J. Pennycook, and S. T. Pantelides, *Phys. Rev. Lett.* **84**, 943 (2000).
- <sup>52</sup>A. Bongiorno and A. Pasquarello, *Appl. Phys. Lett.* **83**, 1417 (2003).
- <sup>53</sup>Jianguo Yu, Susan B. Sinnott, and Simon R. Phillpot (unpublished).